A Method for Distorted Pulse Restoration Based on Frequency Domain Analysis and Transformer Model

De-Jie Chen. Hong-Quan Huang*. Zhong-Lin Wu. Xing-Ke Ma. Qiu-Yi Wang. Zhi-Yong Lan. Li Nie

(College of Nuclear Technology and Automation Engineering, Chengdu University of Technology, Dongsanlu, Erxianqiao, Chengdu, 610059, People's Republic of China)

Abstract

To address the issue of complex distortion in the output signals of the front-end analog system during nuclear pulse signal detection, this paper proposes a distorted pulse restoration method that combines frequency domain analysis with the Transformer model. This method accurately identifies the relevant parameters of nuclear pulse signals through a combination of frequency domain analysis and sample learning, thereby correcting the distorted pulse signals. Initially, pulse signals are analyzed using frequency domain analysis to ascertain the property of the components within the distorted pulses (such as inertial, proportional, and integral components) and the initial parameters of each component. Subsequently, based on the initial parameter ranges of the identified pulse components and predefined mathematical models, multiple datasets comprising distorted pulse sequences are constructed to train the Transformer model. In simulations, the trained model is validated using simulated pulses. Taking distorted first-order, second order, and third-order pulse signals as examples, the corresponding model is employed to identify their amplitudes, and the relative errors are computed. The results indicate that, compared to the case without frequency domain analysis, the incorporation of frequency domain analysis reduces the relative errors in amplitude parameter identification by 0.81%, 0.87%, and 0.77%, respectively. Finally, to further verify the feasibility of combining frequency domain analysis with the Transformer model and assess the model's performance, five X-ray measurements are conducted on a copper ore sample. The measured pulse sequences are digitally processed and used as input to the model. Multi-channel pulse amplitude analysis is then performed on the output pulse amplitudes from the model, yielding an X-ray energy spectrum corrected for shadow peaks. The model's performance is evaluated using the metric R, which represents the proportion of shadow peaks corrected by the model. The results demonstrate that approximately 94.15% of the shadow peaks can be corrected to characteristic peaks. The method proposed in this paper, which combines frequency domain analysis and a transformer model, can effectively restore distorted pulse signals and is of great importance for improving the completeness and resolution of the radiation energy spectrum count.

Keywords: Deep learning. Transformer model. Trapezoidal shaping. Pulse signal restoration.

1. Introduction

In the digital processing and energy spectrum analysis of nuclear pulse signals, trapezoidal shaping emerges as a frequently employed signal processing technique, effectively facilitating the identification of pulse amplitudes. However, the ubiquitous issue of pulse distortion in practical applications poses a severe challenge to the accuracy of these amplitudes. In measurement systems equipped with switch-reset preamplifiers, distorted pulses primarily consist of truncated pulses, which occur when the pulse amplitude abruptly drops to zero due to the switching reset, resulting in pulse signals with insufficient effective width. This distortion problem leads to significant amplitude loss after trapezoidal shaping, ultimately giving rise to shadow peaks near the full-energy peak in the energy spectrum, thereby compromising the counting accuracy and resolution of characteristic peaks.

When applying, various repair methods can be adopted, including deep learning, repair algorithms, etc., to fix distorted pulses. However, when distortion issues arise in complex pulses, the repair difficulty will increase. For instance, in certain nuclear radiation detection applications, the complexity of the front-end analog channel, comprising detectors and conditioning circuits, along with the instability of electronic prat parameters induced by temporal or environmental changes, results in output pulse signals containing multiple components. These components exhibit diverse characteristics in the frequency domain, including proportional, inertial, integral, differential (encompassing first-order or higher-order), and oscillatory components. In the time domain, they manifest as complex waveform features such as exponential signals, step signals, ramp signals, and oscillatory signals. The diversity of pulse components significantly elevates the complexity of the signals. When these pulse components undergo distortion, if they cannot be effectively identified and processed, the task of restoring the distorted pulses becomes even more arduous. Ultimately, this impacts the restoration effectiveness and leads to reduced counting accuracy and resolution of characteristic peaks.

In the field of nuclear signal processing and energy spectrum analysis, an increasing number of researchers are utilizing new algorithms and technologies to address the issues in this domain. Zhang et al. investigated the effect of CR-RC digital filter parameters on nuclear energy spectrum measurements[1] and obtained the optimal parameter. To achieve high count rates, a new true Gaussian digital shaper for detector pulses[2] and a

compensation technology for pulse stacking[3] were proposed. V.T. Jordanov, et al propose efficient digital pulse shaping algorithms[4] for real-time synthesis of multiple pulse shapes. The effect of parameter drift of trapezoidal shaping in nuclear pulse processing is investigated and a correction method[5] is proposed to enhance the system robustness. A bi-exponential signal pulse shaping algorithm[6] is proposed for high count rate environments with improved signal-to-noise ratio and energy resolution. Huang et al. investigated a genetic algorithm-based method[7] for pile-up nuclear pulse parameter estimation.

In addition, deep learning technology has rapidly developed in recent years and demonstrated extensive application potential in the field of nuclear signal energy spectrum analysis. for example, a fast nuclide identification method[8] based on ANN, SVM and other algorithms is proposed to help achieve the fastest identification and classification of gamma and X-ray spectra in nuclear applications. Griffiths et al. used a convolutional neural network[9] to screen neutron-gamma pulses, extracting features directly from the raw data with superior performance in identifying potential substructures of the signal. A method[10] of using a specific NN called U-net as a pulse shaper. It filters the pulses and returns them unfolded, thus solving the stacking problem and even estimating the pulse amplitude when the detector is saturated. Byoungil et al. proposed a deep learning based method[11] for separating and predicting the true pulse height of a signal for application in spectroscopy with a scintillation detector. Deep learning technology provides various ideas for pulse processing in radiation measurement[12][13]. Touch et al. applied an artificial neural network[14] for energy spectrum correction and achieved satisfactory results. Tang Lin et al. proposed using the CNN-LSTM model[15] to identify relevant parameters of distorted pulses and simultaneously achieved energy spectrum correction. Holl, et al. Identification of pulse shapes in germanium detectors by combining a neural network for feature extraction with a smaller classification network[16]. Wang et al. applied the Transformer model to identify pulse[17] parameters. Ai et al. generalized uncertainty estimation of nuclear detector signals[18] based on neural networks and integrated learning. Ma et al. used deep learning CNN-LSTM models for estimating trapezoidal overlapping nuclear pulses[19].

However, for the aforementioned pulse signals with multiple components and complex distortions, a single deep learning model often struggles to fully recognize and effectively process all distortion scenarios. Therefore, this paper proposes an innovative method for restoring distorted pulses, which combines the advantages of frequency domain analysis and the deep learning Transformer model. This method can deeply analyze the complex waveform characteristics of pulse signals, fully recognize and process various distorted components, thereby effectively restoring distorted pulses and improving the accuracy and resolution of nuclear signal energy spectrum analysis. Introducing this technology into the field of nuclear signal energy spectrum analysis is of great significance for enhancing the counting accuracy and resolution of characteristic peaks.

2 Frequency domain analysis and mathematical modeling of pulses

2.1 Frequency domain analysis

The frequency domain analysis method is used to fully identify the components contained in the complex pulses output by the analogue front-end system of a nuclear radiation detector, and to obtain the property and initial parameters of each component. The implementation process is as follows:

Step ①: Randomly select a complete single pulse $h(t)$ from the measured pulses, plot the frequency characteristic trend line of $h(t)$, and calculate the slope of the trend line as well as the coordinates of the intersection points between trend lines, using the following method:

Find the frequency domain expression for $h(t)$ as shown in Eq. (1):

$$H(j\omega) = \int_0^{\infty} h(t) e^{-j\omega t} dt \quad \#(1)$$

Let $\mu = H_0 \ln|H(j\omega)|$, $\gamma = ln\,\omega$, H_0 is a positive constant, plot the $\gamma - \mu$ curve with γ as the horizontal coordinate and μ as the vertical coordinate, and plot the trend line K on the $\gamma - \mu$ curve with n H_0, the trend line is a straight line. Assume the following form of the pulse s-domain obtained from the measurement pulse:

$$G(s) = \frac{K(\tau s + 1)}{(\lambda s + 1)(T_2 s^2 + T_1 s + 1)} \#(2)$$

The individual components included in this are as follows:

one inertial component: $K/(\lambda s + 1)$, component number “1”;

one oscillatory component: $1/(T_2 s^2 + T_1 s + 1)$, with the component number “2”;

one differential component: $(\tau s + 1)$, component number “3”.

The trend lines are shown in Figure 1, and there are 4 trend lines for this pulse. Trend line K1 and the vertical coordinate of the intersection of the coordinates of (γ_0, μ_0), the intersection of the serial number is recorded as "0", the slope is 0; Trend line K1 and the intersection of the trend line K2 coordinates of the intersection of the intersection of the coordinates of the intersection of the intersection of the trend line K1 and the trend line K2 for (γ_1, μ_1) the intersection of the serial number is recorded as "1"; Trend K2 and the Trend K2 and trend line K3 intersection coordinates for (γ_2, μ_2), the intersection number is recorded as "2"; trend line K3 and trend line K4 intersection coordinates for (γ_3, μ_3), the intersection number is recorded as "3".

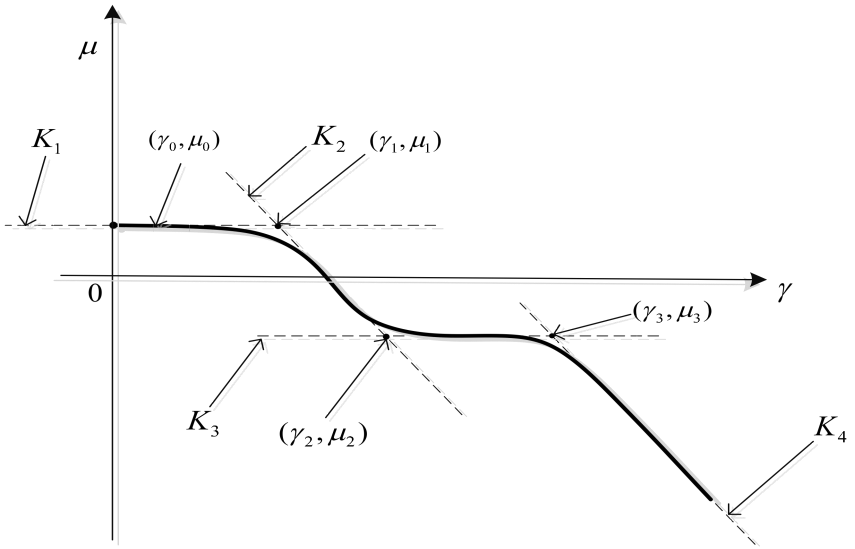

Figure 1 The trend lines

Step② Construct the slope matrix and the component matrix of the trend line, and give the correspondence between the slope matrix, the component matrix and the coordinates of the intersection point in Step ①, and realize it as follows:

The possible slopes of trendline 2, trendline 3, and trendline 4 form the slope matrix U as follows:

$$U = \begin{pmatrix} U_{1,1} & U_{1,2} & U_{1,3} \\ U_{2,1} & U_{2,2} & U_{2,3} \\ U_{3,1} & U_{3,2} & U_{3,3} \\ U_{4,1} & U_{4,2} & U_{4,3} \\ U_{5,1} & U_{5,2} & U_{5,3} \\ U_{6,1} & U_{6,2} & U_{6,3} \end{pmatrix} = \begin{pmatrix} -H_0 & -3H_0 & -2H_0 \\ -H_0 & 0 & -2H_0 \\ -2H_0 & -3H_0 & -2H_0 \\ -2H_0 & -H_0 & -2H_0 \\ H_0 & 0 & -2H_0 \\ H_0 & -H_0 & -2H_0 \end{pmatrix} \#(3)$$

From left to right, the three elements in the same row of matrix U correspond to the slopes of trendline 2, trendline 3 and trendline 4, respectively. Combining the slope characteristics of the three component trend lines and deriving the corresponding component matrices W from the slope matrix U:

$$W = \begin{pmatrix} W_{1,1} & W_{1,2} & W_{1,3} \\ W_{2,1} & W_{2,2} & W_{2,3} \\ W_{3,1} & W_{3,2} & W_{3,3} \\ W_{4,1} & W_{4,2} & W_{4,3} \\ W_{5,1} & W_{5,2} & W_{5,3} \\ W_{6,1} & W_{6,2} & W_{6,3} \end{pmatrix} = \begin{pmatrix} 1 & 2 & 3 \\ 1 & 3 & 2 \\ 2 & 1 & 3 \\ 2 & 3 & 1 \\ 3 & 1 & 2 \\ 3 & 2 & 1 \end{pmatrix} \#(4)$$

where the elements of W are formed by the ordinal numbers of the components.

The correspondence between U, W and intersection points: taking the first row of U as an example, $-H_0$、$-3H_0$and $-2H_0$ correspond to the slopes of the trendline K2, trendline K3 and trendline K4, and correspond to the component numbers 1, 2 and 3 of the first row of W (i.e., inertial, oscillatory and differential components), and correspond to intersections (λ_1, μ_1)、$(\lambda_2, \mu_2)$and(λ_3, μ_3)respectively. This correspondence is summarized as shown in Eq. (5):

$$U_{i,j} \Leftrightarrow W_{i,j} \Leftrightarrow Intersection\ j\ (\gamma_j, \mu_j) \#(5)$$

Step ③ Use the slope of the trendline of pulse $h(t$) and the coordinates of the intersection point in Step ② to find the initial parameter values of the function G(s) as follows (a)~(c):

(a) The inertial component parameters K and λ are solved as follows:

$$\lambda = \frac{1}{e^{\gamma_j}} \#(6)$$

In Eq. (6), "j" denotes the sequence number of the element whose value is "1" in the three elements $W_{i,1}$、$W_{i,2}$ and $W_{i,3}$. And it is obtained from $\mu_0 = H_0 \ln K$:

$$K = e^{\mu_0 / H_0} \#(7)$$

(b) The differential component parameter τ is solved as in Eq. (6).

$$\tau = \frac{1}{e^{\gamma_l}} \#(8)$$

In Eq. (8), "l" denotes the sequence number of the element whose value is "3" in the three elements $W_{i,1}$、$W_{i,2}$ and $W_{i,3}$.

(c) The oscillatory component parameters T_2 and T_1 are solved according to Eq. (9):

$$T_2 = \left(\frac{1}{e^{\gamma_q}}\right)^2 \qquad T_1 = \sqrt{T_2} = \frac{1}{e^{\gamma_q}} \#(9)$$

In Eq. (9), "q" denotes the sequence number of the element whose value is "2" in the three elements $W_{i,1}$、$W_{i,2}$ and $W_{i,3}$.

2.2 pulse mathematical model

2.2.1 pulse model

As mentioned above, due to the complexity of the front-end analog channel composed of the detector and conditioning circuit, as well as the instability of electronic component parameters in the circuit caused by time or environmental changes, the output pulse signal contains multiple components. These components exhibit characteristics such as proportional, inertial, integral, differential, and oscillatory in the frequency domain, and manifest as complex signals such as exponential signals, step signals, ramp signals, and oscillatory signals in the time domain. As shown in Figure 2, these pulse signals can be obtained by connecting the detector output to different circuits (such as RC integrator circuits, differentiator circuits, etc.). Among them, the first stage is the equivalent circuit at the detector output. Each stage is connected through an ideal voltage amplifier, assuming that its input impedance is infinite, output impedance is zero, frequency band is infinitely wide, and voltage gain is 1. Figure 3 presents the s-domain block diagram of the circuit.

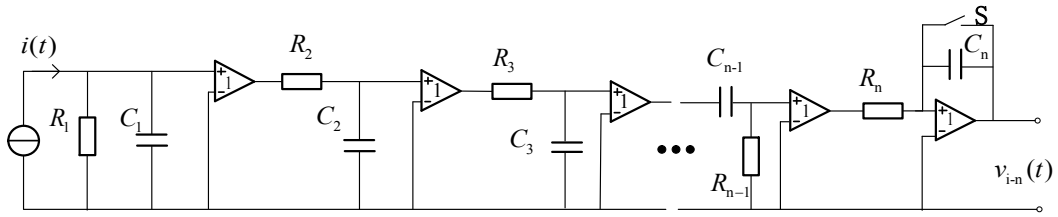

Figure 2 circuit diagram

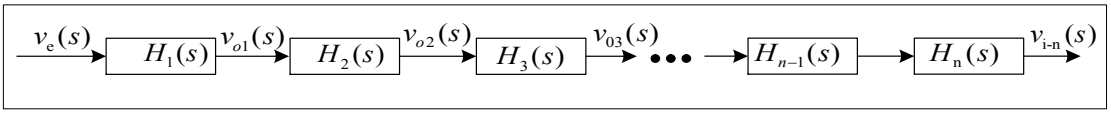

Figure 3 the s-domain block diagram of the circuit

In Figure 3, $v_e(s)$ denotes the detector output, $v_{i\_1}(s)$ is the output signal of the first stage RC circuit, and the simplification of the s-domain block diagram yields $v_{i\_-n}(s)$ (s) as shown in Eq. (10):

$$v_{i-n}(s) = v_e(s)H_1(s)H_2(s)H_3(s)\cdots H_n(s) = \frac{b_m s^m + \cdots + b_1 s + b_0}{a_n s^n + \cdots + a_1 s + a_0} \#(10)$$

This paper takes first-order, second-order, and third-order pulses as examples to derive their mathematical models. Firstly, let $v_{i1}(t)$, $v_{i2}(t)$, and $v_{i3}(t)$ represent the time-domain models of the first-order, second-order, and third-order pulses, respectively. By expanding and simplifying the fraction in Eq. (10), we obtain the output $v_{i3}(s)$ of the third-order RC circuit：

$$v_{i3}(s) = \frac{Q}{C_1}\left(\frac{b s + 1}{(\tau_1 s + 1)(\tau_2 s + 1)(\tau_3 s + 1)}\right) \# = \frac{Q}{C_1}\left(\frac{l_1}{\tau_1 s + 1} + \frac{l_2}{\tau_2 s + 1} + \frac{l_3}{\tau_3 s + 1}\right) \#(11)$$

In Eq. (11): $\tau_1 = R_1 C_1$, $\tau_2 = R_2 C_2$, $\tau_3 = R_3 C_3$, and Q is the lectric charge. $l_1 = f(\tau_1, \tau_2, \tau_3)$, $l_2 = f(\tau_1, \tau_2, \tau_3)$, $l_3 = f(\tau_1, \tau_2, \tau_3)$. Let b=0, and then inverse transform Eq. (11) to obtain the third-order pulse time-domain mathematical model $v_{i3}(t)$:

$$v_{i3}(t) = A\left(k_1 e^{-t/\tau_1} + k_2 e^{t/\tau_2} + k_3 e^{-t/\tau_3}\right) \#(12)$$

Discretization of Eq. (12) leads to a third-order pulse digitization model:

$$v_{i3}(n T_{clk}) = A\left(k_1 e^{-n T_{clk}/\tau_1} + k_2 e^{-n T_{clk}/\tau_2} + k_3 e^{-n T_{clk}/\tau_3}\right) \#(13)$$

In Eq. (13): $k_1 = \tau_1/((\tau_2 - \tau_1)(\tau_3 - \tau_1))$, $k_2 = \tau_2/((\tau_1 - \tau_2)(\tau_3 - \tau_2))$, $k_3 = \tau_3/((\tau_1 - \tau_3)(\tau_2 - \tau_3))$, where τ_1, τ_2, τ_3 and τ_3 are unequal to each other; A is the pulse amplitude coefficient of the third order, $A = Q/C_1$; T_{clk} is the sampling period.

From Eq. (12), when $k_1 = 1$, $k_2 = 0$、$k_3 = 0$, the first-order pulse time-domain expression $v_{i1}(t)$ and the digitized model $v_{i1}(n T_{clk})$ can be obtained as follows:

$$v_{i1}(t) = A e^{-t/\tau} \#(14)$$

$$v_{i1}(n T_{clk}) = A e^{-n T_{clk}/\tau} \#(15)$$

In Eq. (14): A is the first-order pulse amplitude coefficient, τ is the time constant, and T_{clk} is the sampling period.

From Eq. (12), when $k_1 = 1$, $k_2 = 0$, the second-order pulse time-domain expression $v_{i2}(t)$ and the digitized model $v_{i2}(n T_{clk})$ can be obtained as follows:

$$v_{i2}(t) = A\left(k_1 e^{-t/\tau_1} + k_2 e^{-t/\tau_2}\right) \#(16)$$

$$v_{i2}(n T_{clk}) = A\left(k_1 e^{-n T_{clk}/\tau_1} + k_2 e^{-n T_{clk}/\tau_2}\right) \#(17)$$

In Eq. (16): A is the second-order pulse amplitude coefficient, when k_2 is negative, $\tau_1 > \tau_2$, in this paper for the experimental simulation of k_1 take the value of 1 , k_2 take the value of -1, at this time, τ_1 for the slow time constant, τ_2 for the fast time constant, T_{clk} is the sampling period.

2.2.2 pulse digital shaping model

In the context of digital shaping of nuclear pulses, trapezoidal shaping assumes a significant role, serving as a replacement for complex analog filter shaping circuits. The high signal-to-noise ratio performance of the pulses post-filtering, coupled with the capacity to adjust the pulse width and flat-top width of the output waveform by tuning the shaping parameters, renders trapezoidal shaping a prevalent component in digital measurement systems. The time-domain expression for the trapezoidal pulse is given by Eq. (18):

$$v_o(t) = \sum_1^4 y_i(t) = \begin{cases} y_1(t) = (y_m / t_a) t\, u(t) \\ y_2(t) = -y_1(t - t_a) u(t - t_a) \\ y_3(t) = -y_1(t - t_b) u(t - t_b) \\ y_4(t) = y_1(t - t_c) u(t - t_c) \end{cases} \#(18)$$

In the equation given by (18), the symbol y_m denotes the flat-top amplitude of the trapezoidal pulse, t_a signifies the rise time of the trapezoidal pulse, t_c designates the shaping time of the trapezoidal pulse, $t_b - t_a$ indicates the duration of the flat-top of the pulse, and $u(t)$ is the ideal step function. Subsequent to performing the z-transform on $v_o(t)$, the following result is obtained:

$$v_o(z) = \frac{y_m z\left(1 - z^{-n_a} - z^{-n_b} + z^{-n_c}\right)}{n_a (z-1)^2} \#(19)$$

In Eq. (19): $n_a = t_a / T_{clk}$, $n_b = t_b / T_{clk}$, $n_c = t_c / T_{clk}$, and $n_c = n_a + n_c$; T_{clk} is the sampling period.

(1) Trapezoidal shaping of first-order pulse

The z-domain expression for the pulse of first order is obtained by transforming Eq. (14) by z as follows:

$$v_{i1}(z) = \frac{A z}{z - e^{-T_{clk}/\tau}} \#(20)$$

The transfer function $H(z)$ for the first-order pulse trapezoidal shaping transform can be obtained by associating Eqs. (19) and (20) as follows：

$$H(z) = \frac{v_o(z)}{v_{i1}(z)} = \frac{y_m z\left(1 - z^{-n_a} - z^{-n_b} + z^{-n_c}\right)}{n_a (z-1)^2} \Bigg/ \frac{A z}{z - e^{-T_{clk}/\tau}}$$
$$= \frac{y_m z\left(1 - z^{-n_a} - z^{-n_b} + z^{-n_c}\right)}{A n_a (1 - z^{-1})^2} \#(21)\#$$

Cross-multiplying both sides of Eq. (21) equation and further simplifying using the inverse transformation of z yields the following recursive formula for first-order pulse trapezoidal shaping:

$$v_o[n] = 2v_o[n-1] - v_o[n-2]$$
$$+ \frac{\gamma}{n_a}\{v_{i1}[n-1] - v_{i1}[n-n_a-1] - v_{i1}[n-n_b-1] + v_{i1}[n-n_c-1]\}$$
$$- \frac{\gamma e^{-T_{clk}/\tau}}{n_a}\{v_{i1}[n-2] - v_{i1}[n-n_a-2] - v_{i1}[n-n_b-2] + v_{i1}[n-n_c-2]\} \#(22)$$

In Eq. (22): γ is the proportionality coefficient between the trapezoidal amplitude y_m and the first-order pulse amplitude coefficient A, γ=1, and T_{clk} is the sampling period.

(2) Trapezoidal shaping of second-order pulse

Similarly, the z-transformation of Eq. (16) and the simultaneous coupling of Eq. (19) leads to a recursive equation for trapezoidal shaping of second-order pulses as follows：

$$v_o[n] = 2v_o[n-1] - v_o[n-2]$$
$$+ \frac{\gamma}{n_a (e^{-T_{clk}/\tau_1} - e^{-T_{clk}/\tau_2})}\{v_{i2}[n] - v_{i2}[n-n_a] - v_{i2}[n-n_b] + v_{i2}[n$$
$$- \frac{\gamma (e^{-T_{clk}/\tau_1} + e^{-T_{clk}/\tau_2})}{n_a (e^{-T_{clk}/\tau_1} - e^{-T_{clk}/\tau_2})}\{v_{i2}[n-1] - v_{i2}[n-n_a-1] - v_{i2}[n-n_b-1] + v_{i2}[n$$
$$+ \frac{\gamma (e^{-T_{clk}/\tau_1} e^{-T_{clk}/\tau_2})}{n_a (e^{-T_{clk}/\tau_1} - e^{-T_{clk}/\tau_2})}\{v_{i2}[n-2] - v_{i2}[n-n_a-2] - v_{i2}[n-n_b-2] + v_{i2}[n$$

In Eq. (23): γ is the proportionality coefficient between the trapezoidal amplitude y_m and the second-order pulse amplitude coefficient A, γ =1, and T_{clk} is the sampling period.

(3) Trapezoidal shaping of third-order pulse

Similarly, the z-transformation of Eq. (13) and the simultaneous coupling of Eq. (19) leads to a recursive equation for trapezoidal shaping of third-order pulses as follows：

$$-N_1 v_o[n] + (2N_1 + N_2)v_o[n-1] - (N_1 + 2N_2)v_o[n-2] + N_2 v_o[n-3]$$
$$= \frac{\gamma}{n_a}\{v_{i3}[n] - v_{i3}[n-n_a] - v_{i3}[n-n_b] + v_{i3}[n-n_c]\}$$
$$- \frac{\gamma (d_1 + d_2 + d_3)}{n_a}\{v_{i3}[n-1] - v_{i3}[n-n_a-1] - v_{i3}[n-n_b-1] + v_{i3}[n-n_c-1]\}$$
$$+ \frac{\gamma (d_1 d_2 + d_1 d_3 + d_2 d_3)}{n_a}\{v_{i3}[n-2] - v_{i3}[n-n_a-2] - v_{i3}[n-n_b-2] + v_{i3}[n-n_c-2]\}$$
$$- \frac{\gamma (d_1 d_2 d_3)}{n_a}\{v_{i3}[n-3] - v_{i3}[n-n_a-3] - v_{i3}[n-n_b-3] + v_{i3}[n-n_c-3]\} \#(24)$$

In Eq. (24): $d_1 = e^{-T_{clk}/\tau_1}$, $d_2 = e^{-T_{clk}/\tau_2}$, $d_3 = e^{-T_{clk}/\tau_3}$; T_{clk} is the

sampling period; $N_1 = k_1(d_2 + d_3) + k_2(d_1 + d_3) + k_3(d_1 + d_2)$, $N_2 = k_1 d_2 d_3 + k_2 d_1 d_3 + k_3 d_1 d_2$; γ is the proportionality coefficient between the trapezoidal amplitude y_m and the third-order pulse amplitude coefficients A, γ=1.

In summary, a digital model for the pulse and a trapezoidal shape expression $v_o[n]$ have been derived. $v_o[n]$ will be used as an input to the deep learning model.

3 Principles and methods

3.1 Frequency domain analysis and Transformer model principle analysis

To address the complex distortion of output signals from the front-end analog system in nuclear pulse signal detection, this study employs a method that combines frequency domain analysis (hereinafter referred to as FDA) with the deep learning Transformer model. The implementation process is as follows:

(1) The nuclear pulse signals output by the front-end analog system are analyzed using FDA to determine the property of the components contained in the pulse (such as differentiation, inertia, proportion, integration, and oscillation), and the initial parameter values of each component are calculated.

(2) Based on the property of the pulse components and the range of their initial parameter values, hierarchical training is conducted to obtain different Transformer models.

(3) The measured distorted pulse signals are converted into digital signals X(n) through a conditioning circuit.

(4) The digital signals X(n) undergo digital waveform shaping to yield Y(n).

(5) Depending on the range of initial parameter values obtained in (1) and the property of the components contained in the distorted pulse, Y(n) is fed into a specific submodule within the corresponding Transformer model for parameter identification, thereby obtaining more accurate parameters such as pulse amplitude. The flowchart for the restoration of complex distorted nuclear pulse signals is shown in Figure 4.

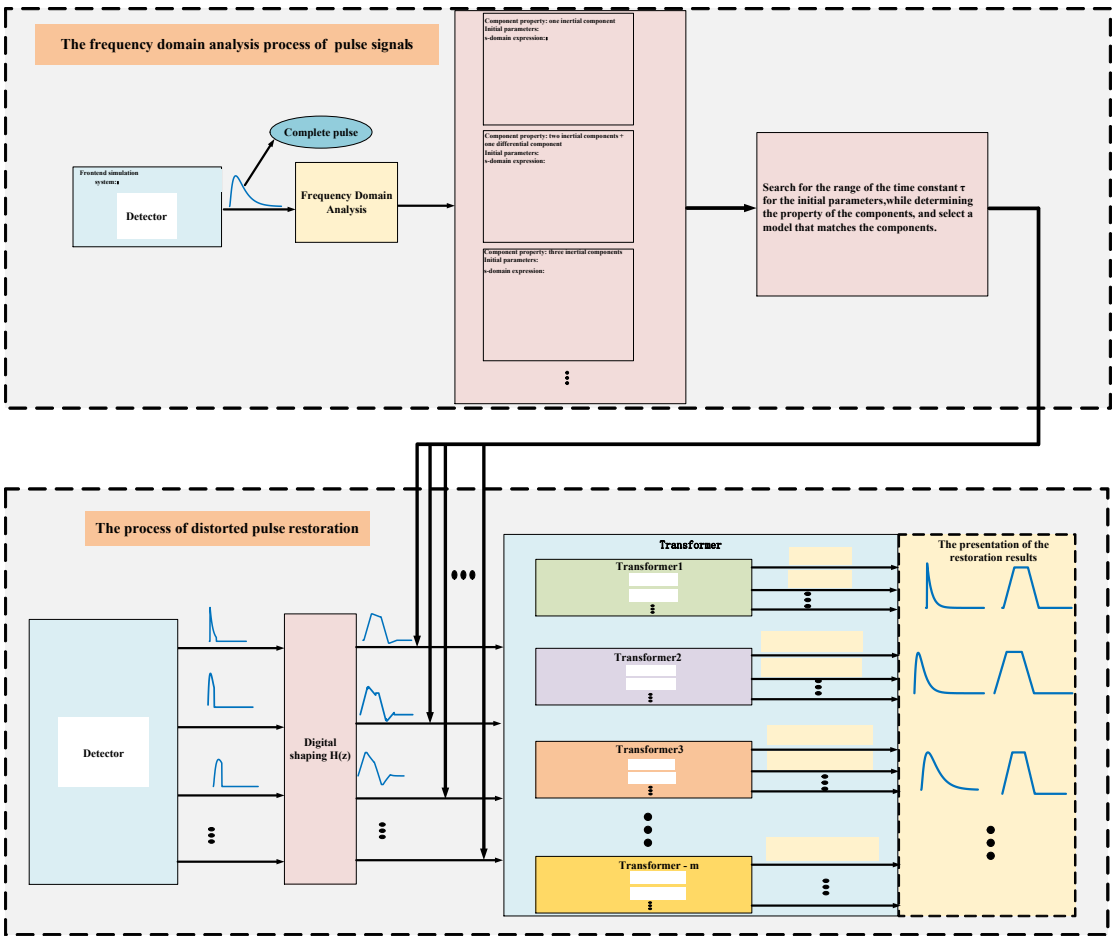

Figure 4 The flowchart for the restoration of complex distorted nuclear pulse signals

By integrating frequency domain analysis with a hierarchical Transformer model architecture, complex distorted pulses are processed to achieve the restoration of distorted pulse signals. The specific working principle is as follows:

Taking the first-order pulse signal shown in Figure 4 as an example, the process initiates with the application of frequency domain analysis to identify the components within the nuclear pulse, yielding the first-order pulse and its initial parameter value τ_0'. Subsequently, a digital shaping technique is employed to apply trapezoidal shaping to the distorted first-order pulse $X_1(n)$, resulting in the trapezoidal pulse $Y_1(n)$. Finally, based on the property of $Y_1(n)$ (the trapezoidal shaping outcome of the first-order pulse) and the range of τ_0', it is routed to the first-layer model (Transformer1', Transformer1", etc.) for further processing. However, the specific sub-model within the first layer that is selected depends on the range in which the initial value τ_0' falls, determined by whether $\tau_0' \subseteq \tau$, where τ is the time constant used during model training. This approach significantly enhances the accuracy of the model, as it focuses on analyzing pulses with specific characteristics and within a narrow parameter range, thereby reducing the complexity of processing distorted pulses and improving the model's precision.

As mentioned above, during the model training phase, different models are trained based on the property of the pulses and the range of their initial parameter values. Therefore, when constructing the dataset, this paper generates distinct datasets according to the range of the initial value τ_0' of the first-order pulses, which are then used to train different Transformer models. For instance, when training Transformer models for first-order pulses, the relationship between different models and their corresponding datasets is illustrated in Figure 5: the dataset for the Transformer1' model covers a time constant τ range of [3.2, 5.0] μs; whereas, the dataset for the Transformer1" model spans a time

constant τ range of [6.0, 10.0] μs. During model invocation, if τ_0' = 3.8 μs, the Transformer1' model is selected; if τ_0' = 7.9 μs, the Transformer1' model is chosen; and so forth. This approach narrows down the search range for the pulse parameter τ_0', enabling the selection of an appropriate Transformer model for analysis, thereby significantly enhancing the accuracy of the model.

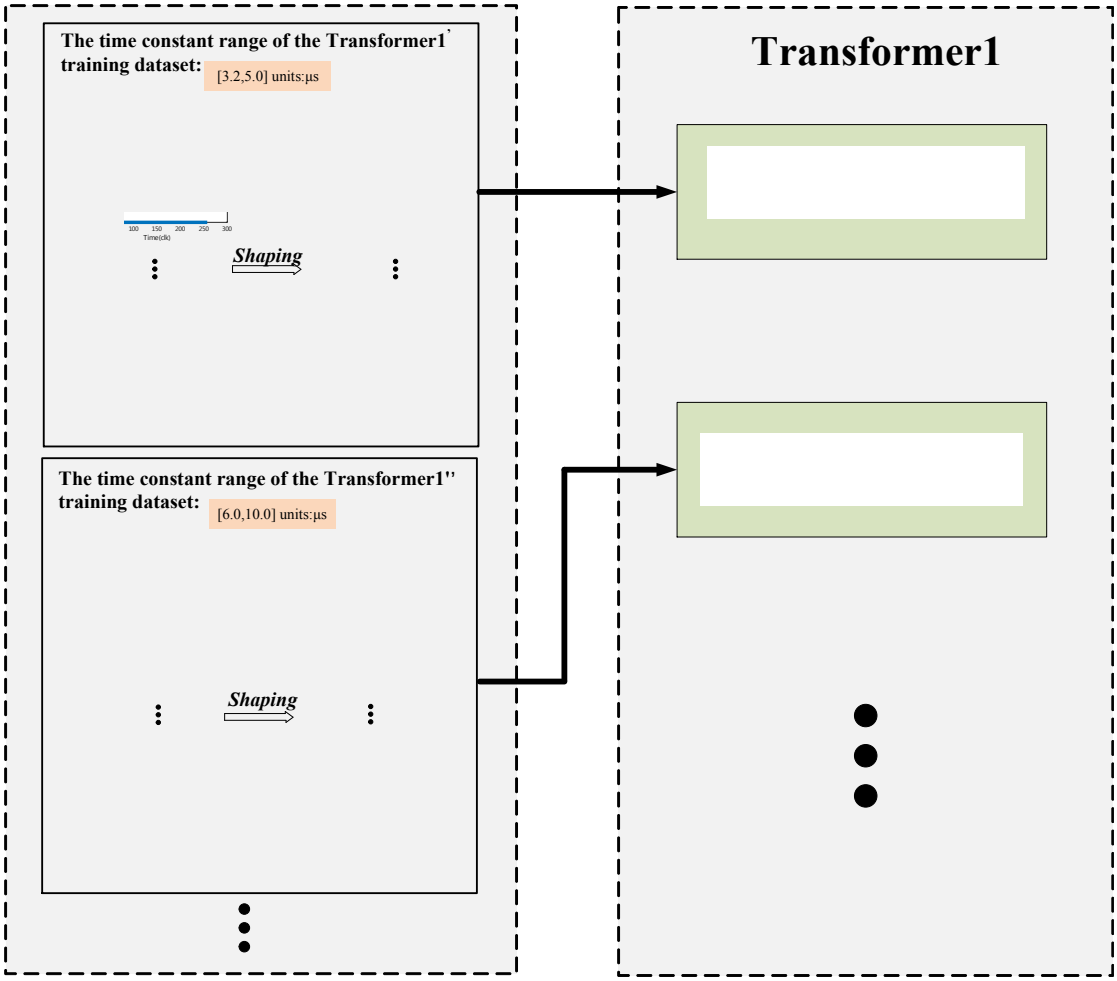

Figure 5 Relationship between datasets and models with different time constants

3.1.1 Transformer model feasibility analysis

Nuclear pulse signals are digitally processed to convert them into waveforms with specific characteristics. As shown in equation (24), a third-order pulse can be transformed into a trapezoidal pulse, suggesting a complex fitting relationship between the trapezoidal pulse and the shaping parameters A, $\tau_1, \tau_2, \tau_3, t_r$ and t_f. These parameters can be accurately identified using fitting algorithms, such as deep learning neural network models, to restore distorted pulse signals. (Here, $t_r = t_a$, $t_f = t_b - t_a$, where t_r and t_f represent the rise time and flat-top duration of the trapezoidal shaping, respectively; τ denotes the time constant, and A represents the pulse amplitude coefficient).

The Transformer model, with its powerful sequence processing and feature extraction capabilities, can effectively identify the trapezoidal shaping parameters of pulse signals, thereby restoring distorted pulses. Therefore, the core of addressing the distorted pulse problem lies in using the model to identify the trapezoidal shaping parameters of the pulse and using these parameters to replace the parameters of the original distorted pulse, thus achieving pulse restoration. The specific implementation steps include: dataset construction (generating a pulse sequence dataset containing different shaping parameters for distorted pulses), forward propagation computation (extracting features of the pulse signals and identifying their shaping parameters through the transformer model), and backward propagation computation (optimizing model parameters using error backpropagation to improve identification accuracy).

3.2 Dataset

Taking the third-order pulse as an example, the dataset used for the Transformer model in this paper is composed of the sampled values $V_o(m \times T_{clk})$ of the trapezoidal pulse obtained after trapezoidal shaping of the distorted pulse, along with its corresponding set of trapezoidal shaping parameters. Let P_i denote the set of trapezoidal shaping parameters, which is derived from the relevant parameters of the distorted pulse and the timing parameters associated with its trapezoidal shaping. Taking the ith parameter set P_i as an example, this set includes the pulse amplitude A_i (where i = 1, 2, ..., N), time constants τ_1, τ_2, τ_3, as well as the rise time t_r and the flat-top duration t_f of the trapezoidal shaping. The dataset can be represented in matrix form as follows:

$$\begin{bmatrix} [V_o(T_{clk})]_1 & [V_o(2 \times T_{clk})]_1 & \cdots & [V_o(m \times T_{clk})]_1 & P_1 \\ [V_o(T_{clk})]_2 & [V_o(2 \times T_{clk})]_2 & \cdots & [V_o(m \times T_{clk})]_2 & P_2 \\ \vdots & & \ddots & \vdots & \\ [V_o(T_{clk})]_N & [V_o(2 \times T_{clk})]_N & \cdots & [V_o(m \times T_{clk})]_N & P_N \end{bmatrix} \#(25)$$

The dataset (25) comprises N samples of distorted pulses, with each row representing the data of a sample. The initial m columns of data in each sample correspond to the sampled values of the corresponding trapezoidal shaping pulse for the sample, and the final column represents the set of trapezoidal shaping parameters. This parameter set can be expressed as $P = [A_1, A_2, \ldots, A_N, \tau_1, \tau_2, \tau_3, t_r, t_f]$.It should be noted that, as previously mentioned, τ_1, τ_2 and τ_3 are all controlled to be within a small range when creating the dataset.

The dataset is divided into a training set and a validation set with a ratio of 8:2. The training set is used to train the model and determine parameters such as weights and biases. The validation set, on the other hand, is not involved in the training process and is only used to adjust hyperparameters of the model, such as the number of training epochs and the learning rate. A sufficient test set is also prepared under the same conditions to evaluate the model's performance after training. When creating the dataset, the trapezoidal shaping results of three types of distorted pulses (first-, second-, and third-order) are shown in Figure 6. Before the pulses become distorted, the amplitudes of the trapezoidal shaping results for all three types of pulses are 150 mV. After distortion, a common feature can be observed in the three trapezoidal pulses: a significant loss in the amplitude of the shaping results.

(a) (b) (c)

Figure 6 Distorted pulse and trapezoidal shaping result

3.3 Forward propagation

During the forward propagation of the model, the sampled values of the trapezoidal pulses from the training set, denoted as $V_o(m \times T_{clk})_i$, are processed through positional encoding and then fed into the encoder as input. The encoder calculates global dependencies through the attention mechanism, extracts sequence features, and sequentially passes them to the normalization residual connection module and the feedforward network. Ultimately, the output is generated through a linear layer: the set of trapezoidal shaping parameters P'. Unlike traditional RNNs, the Transformer processes sequences based on the attention mechanism without relying on recursive relationships between time steps. Since the Transformer processes the sequence as a whole, it can fully leverage parallel computing, significantly reducing training time and enhancing its ability to model long sequences. In addition, positional encoding is a crucial part of the input stage. It provides the model with sequence order information through sine and cosine functions, thereby compensating for the Transformer's insensitivity to sequence order.

(1) Positional Encoding

In the Transformer architecture, since recurrent neural networks or convolutional neural networks are not used, positional information within the sequence cannot be directly utilized. Therefore, to enable the model to learn information about various positions in the sequence, the Transformer employs positional encoding. The positional encoding is calculated as follows:

$$PE_{(pos,2j)} = sin\left(pos/10000^{2j/d_m}\right) \#(26)$$

$$PE_{(pos,2j+1)} = cos\left(pos/10000^{2j+1/d_m}\right) \#(27)$$

In Eqs. (26) and (27), *pos* represents the position of the information in the sequence, $PE_{(pos,2j)}$ and $PE_{(pos,2j+1)}$ denote the encodings of position *pos* in the 2*j*-th and (2*j*+1)-th dimensions, respectively, and d_m represents the embedding dimension.

Let the input to the model be *X*. Then *X* is obtained by adding the trapezoidal pulse sequence $V_o(m \times T_{clk})$ and the positional encoding *PE* of the pulse sequence. That is, after positional encoding, the expression for the input sequence *X* to the model is as follows:

$$X_{(i,2j)} = \left[V_o\left(2jT_{clk}\right)\right]_i + PE_{(pos,2j)} \#(28)$$

$$X_{(i,2j+1)} = \left[V_o\left((2j+1)T_{clk}\right)\right]_i + PE_{(pos,2j+1)} \#(29)$$

(2) Self-attention mechanism

The core of the Transformer model is the self-attention mechanism. This mechanism calculates the relevance weights of each element with respect to other elements in the sequence, and then uses these weights to compute the weighted sum for each element. The use of the self-attention mechanism not only increases computational efficiency, but also allows for a better capture of the correlations between elements.

Given the sequence *X* obtained after positional encoding of the trapezoidal pulse sampled values, in the self-attention mechanism, for each input sequence *X*, three different linear transformations are first applied to compute the query vector *Q*, the key vector *K*, and the value vector *V*. This linear transformation process can be expressed as:

$$Q = W_Q X, \quad K = W_K X, \quad V = W_V X \#(30)$$

Here, W_Q、W_K and W_V are the weight matrices for model training.

Then, the attention weights are calculated by dot product, and the final output of the self-attention mechanism weights is shown in Equation (31):

$$Attention(Q,K,V) = softmax\left(\frac{QK^T}{\sqrt{d_k}}\right)V \#(31)$$

where d_k is the dimension of the vector K, and Q, K and V represent the data vectors of the input sequence X mapped to query, key and value respectively.

(3) Multi-Head Attention

The multi-head attention mechanism can be understood as a mechanism that maps the original sets of Q (query), K (key), and V (value) vectors into h subspaces and independently computes attention weights in each subspace. Specifically, the Q, K, and V vectors, obtained from the input sequence X through Equation (31), are linearly transformed into vectors in h subspaces, respectively. Then, dot-product attention weights are computed separately in each subspace. Finally, the attention information obtained from each subspace is concatenated and passed through another linear transformation to yield the final output vector of the multi-head attention layer. The multi-head attention mechanism is calculated as follows:

$$MHA(X) = Concat(head_1, \cdots, head_h)W^0 \#(32)$$

$$where\ head_i = Attention\left(QW_i^Q, KW_i^K, VW_i^V\right) \#(33)$$

Here, W_i^Q、W_i^K and W_i^V represent the linear projection parameter matrices for the i-th head, W^0 represents the parameter matrix for the output projection, and headi denotes the self-attention distribution of the i-th head.

(4) Feed-Forward Neural Network

In the Transformer model, the Feed-Forward Network (FFN) receives the output from the Multi-Head Attention (MHA) mechanism and Layer Normalization as its input. It then maps this input to a new representation vector through two linear transformations followed by a nonlinear activation function. Assuming x_0 is the output obtained from the input sequence X after processing through the multi-head attention layer and the normalized residual connection, the computation process of the feed-forward network can be expressed expressed as:

$$FFN(x_0) = \max[0, x_0 W_1 + b_1] W_2 + b_2 \#(34)$$

where W_1 and W_2 represent two different sets of weights, and b_1 and b_2 are the two bias parameters.

（5）Normalization and Residual Connections

The data passing through the multi-head attention or feed-forward network in a Transformer model is not directly used as the output. Instead, it undergoes normalization and residual connections for further processing. The primary purpose of normalization is to prevent gradient vanishing and gradient explosion, thereby accelerating training speed and enhancing training stability. The addition of residual connections helps address the degradation problem in neural networks. Let x be the output obtained after processing the input sequence X through the feed-forward neural network layer and the normalization with residual connections. The mathematical model for normalization and residual connections can be expressed as:

$$x_0 = LayerNorm(X + MHA(X)) \#(35)$$
$$x = LayerNorm(x_0 + FFN(x_0)) \#(36)$$

Here, x_0 represents the result after multi-head attention and normalization; MHA(X) and FFN(x_0) denote the outputs of the multi-head attention and feed-forward network, respectively.

(6) Linear layer

Finally, a linear layer is applied to map the high dimensional features from the Transformer encoder to the values of the pulse trapezoidal shaping parameters, resulting in the trapezoidal shaping parameter set P'.This output layer is implemented using a linear transformation and its mathematical expression is as follows：

$$P' = W * x + b \#(37)$$

where W represents the weight matrix, b is the bias vector, x is the output vector from the Transformer encoder, and P' is the final predicted set of pulse parameters. In summary, the forward propagation calculation process is shown in Figure 7:

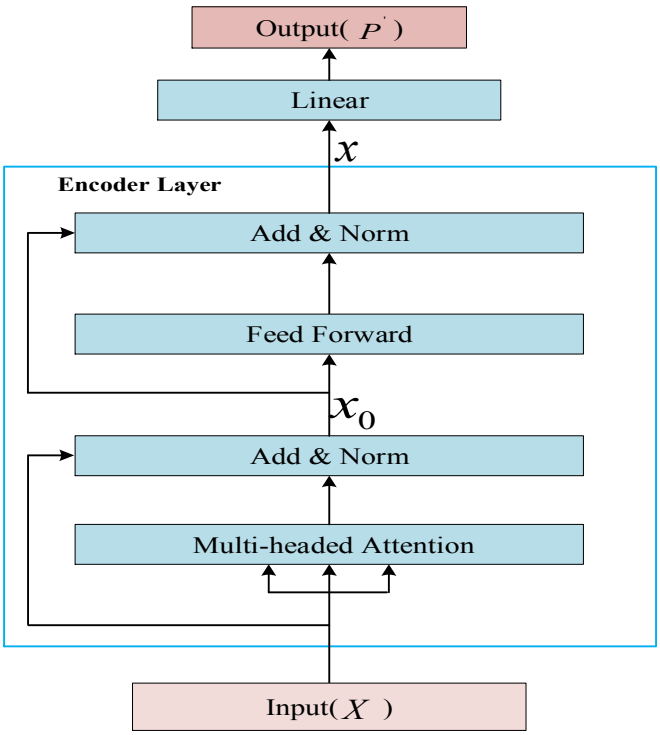

Figure 7 Forward propagation calculation process

3.4 Backpropagation

In the Transformer model, the initial values of the three matrices W_Q, W_K, and W_V corresponding to the input sequence X are randomly initialized. During each forward propagation, the model's output (i.e., the set of predicted trapezoidal shaping parameters P'_i) is computed and compared to the actual set of trapezoidal shaping parameters P_i from the training set to obtain the loss value (or error). Therefore, during the backpropagation process, the error is calculated using the loss function, and the gradients of the model parameters (W_Q, W_K, and W_V) are updated based on this error. This allows the model to gradually reduce the error and improve prediction accuracy in subsequent iterations. For a training set comprising M samples, the Mean Absolute Error (MAE) of the parameter set P_i is used as the value of the loss function, which is calculated as follows:

$$Loss_{MAE} = \frac{1}{M}\sum_{i=1}^{M}\left|P'_i - P_i\right| \#(38)$$

In summary, the network architecture of the Transformer, as illustrated in Figure 8, includes the input layer, various encoder sublayers, the output layer, and the backpropagation structure.

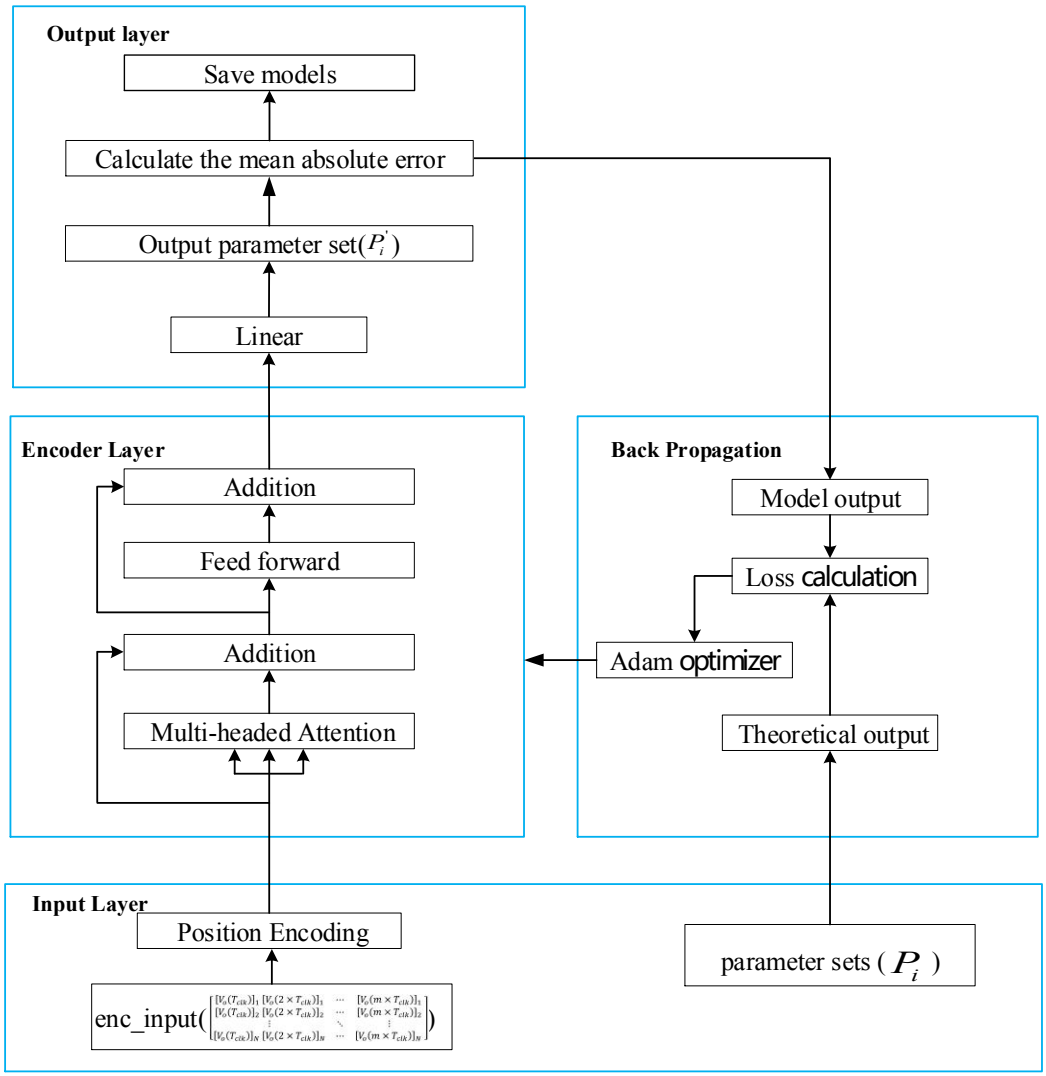

Figure 8 The network architecture of the Transformer

3.5 model training

As mentioned above, in order to investigate the effectiveness of the combined method of Frequency Domain Analysis (hereafter abbreviated as FDA) and the Transformer model in identifying parameters related to distorted pulses, this study performed classification training on the three types of distorted pulses mentioned above (first, second and third order pulses) along with their initial parameter value ranges. This resulted in three transformer models with different parameter configurations, named Transformer1, Transformer2 and Transformer3, each consisting of several sub-models. These three models were trained using the Adam optimizer, and the key hyperparameter configurations for some of the models are shown in:

Table 1 Key hyperparameter configurations of the model

Types of Hyperparameters	Transformer1(first-order pulse)	Transformer2(second-order pulse)	Transformer3(third-order pulse）
Embedding Dimension	512	512	512
Number of Encoder Layers	2	2	2
Number of Attention Heads	16	16	16
FNN Hidden Layer Dimension	2048	2048	2048
Dimension of QKV (Query, Key,	32	32	64

Value) Vectors			
Initial Learning Rate	0.0001	0.0001	0.00001
Batch Size	32	32	48

After training, the loss function iterations of the training and validation sets for each of the three sub models taken from the three transformer models are shown in Figure 9: Figure 9.a shows the values for Transformer1', Figure 9.b shows the loss values for Transformer2', and Figure 9.c shows the loss values for Transformer3'.

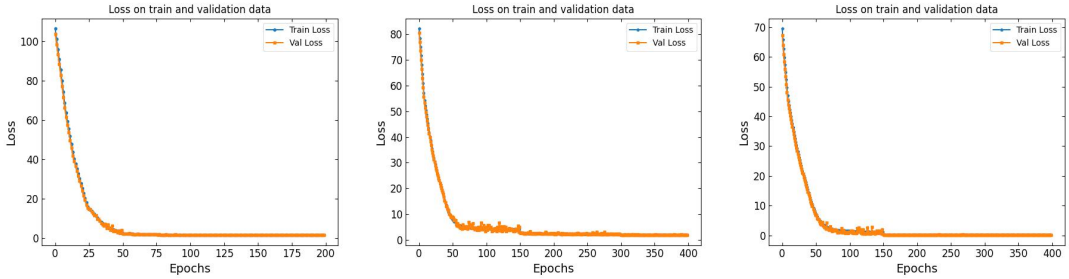

(a) (a) (c)

Figure 9 Train and validate loss values

As can be seen in Figure 9, as the number of training cycles increases, the loss values of the training and validation sets of the three models show a downward trend, with some minor fluctuations in between, and eventually tend to stabilize. This indicates that the model is not overfitting and therefore does not require a separate dropout layer.

3.6 Simulation verification and experiments

3.6.1 Restoration of first-order distortion pulses

Taking the two distorted output pulses from Eq. (14) as an example, they are denoted as pulse 1 and pulse 2. It is assumed that the amplitude coefficient A of the pulse to be restored is 300 mV, with time constants τ of 3.6 μs and 7.4 μs respectively. At the same time, two sub-models, denoted Transformer1' and Transformer1", are extracted from the first-layer model. These sub-models are trained using time constant ranges of [3.2, 5.0] μs and [6.0, 10] μs, respectively. The trapezoidal shaping results of distorted Pulse 1 and Pulse 2 are then fed into these two sub-models for analysis.

Figure 10 shows a comparison between the two original first order distorted pulses and the pulses identified and restored by each model. Table 2 shows a comparison of the true pulse amplitude parameters and the pulse amplitude parameters identified by each sub model, both before and after the incorporation of frequency domain analysis (FDA). The comparison shows that the average relative error of the pulse amplitude coefficients is 1.02% before the application of FDA, whereas it is reduced to 0.21% after the application of FDA. This shows that FDA can accurately select the model that corresponds to the range of pulse parameter values, thereby allowing more accurate identification of the pulse parameters.

Table 2 Comparison of the parameters of the original first-order pulse and the recognition pulse

	Pulse sequence number	Model	Parameter	True pulse amplitude	Identification value	Relative error /%
Before	1	*Transformer* 1"	A	300	297.35	0.88
	2	*Transformer* 1'	A	300	296.51	1.16
After	1	*Transformer* 1' +FDA	A	300	299.17	0.27
	2	*Transformer* 1"	A	300	300.42	0.14

+FDA

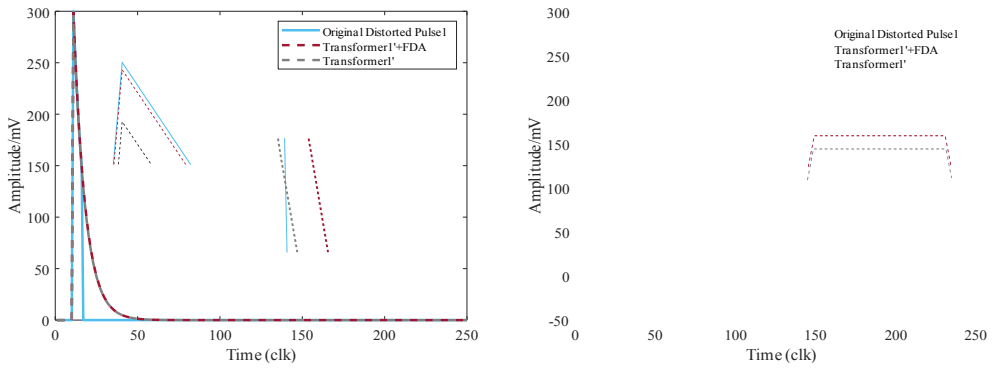

(a)

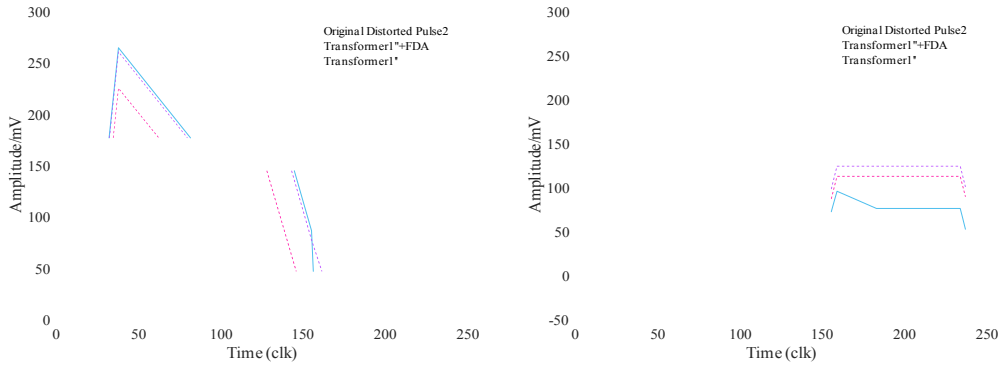

(b)

Figure 10 Comparison of the original first-order distortion pulse and the pulse after recognition and restoration

3.6.2 Restoration of second-order distortion pulses

In the experiment described in Section 3.6.1, we analyzed first-order distorted pulses and verified the feasibility of combining frequency domain analysis with the Transformer model. Now, we will conduct an experiment using two second-order distorted pulses generated by Eq. (16). The relevant parameters of the two pulses are presented in Table 3.

Table 3 Pulse-related parameters

Parameters	Pulse 1	Pulse 2
A(mV)	300	300
$\tau_1(\mu s)$	4.0	6.2
$\tau_2(\mu s)$	1.8	2.1

Simultaneously, two sub-models are selected from the second-layer model: the Transformer2' model, trained with time constant ranges of $3.2 \le \tau_1 \le 5.0$ and $1.2 \le \tau_2 \le 2.8$, and the Transformer2'' model, trained with time constant ranges of $5.2 \le \tau_1 \le 6.8$ and $2.0 \le \tau_2 \le 2.8$; the unit for these time constants is μs. The trapezoidal shaping results of distorted Pulse 1 and Pulse 2 are then fed into these two sub-models for analysis. Figure 11 presents a comparison between the original second-order distorted pulses and the pulses identified and restored by each model. Table 4 compares the true amplitude parameters of the pulse before and after the addition of frequency domain analysis with the pulse amplitude parameters identified by each sub model. Before the addition of the frequency domain analysis (FDA), the average relative error of the pulse amplitude coefficient was 1.22%; after the addition of the frequency domain analysis (FDA), the average relative error of the pulse amplitude coefficient was 0.35%.

Table 4 Comparison of parameters between the original second-order pulse and the identified pulse

	Pulse sequence number	Model	Parameter		True pulse amplitude	Identification value	Relative error /%
Before	1	$Transformer2''$	A		300	296.82	1.06
	2	$Transformer2'$	A		300	304.16	1.38
After	1	$Transformer2'$ +FDA	A		300	298.85	0.38
	2	$Transformer2''$ +FDA	A		300	299.07	0.31

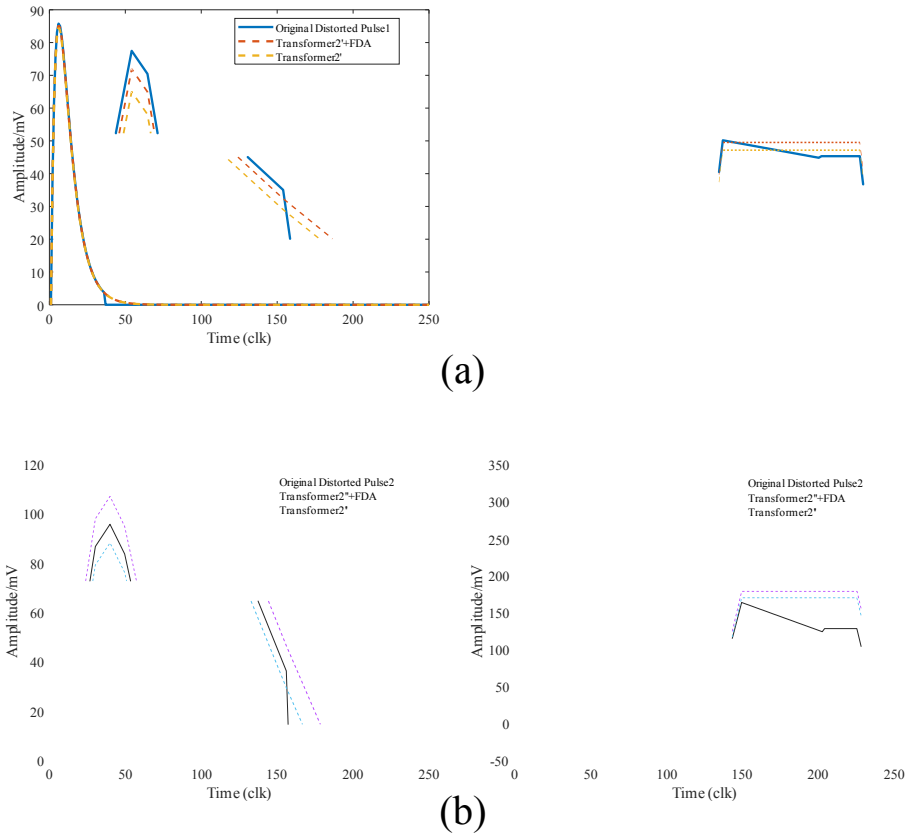

Figure 11 Comparison of the original second-order distortion pulse and the pulse after recognition and restoration

3.6.3 Restoration of third-order distortion pulses

For the restoration of distorted third-order pulses, more parameters need to be identified, placing higher demands on the model. Directly identifying pulses over a wide range would increase the difficulty of identification and make it hard to achieve satisfactory results. Therefore, the introduction of frequency domain analysis significantly narrows the pulse search range and enables the model to achieve better identification performance within each smaller range. To further verify the feasibility of combining frequency domain analysis with Transformer for distorted third-order pulses, two such pulses are selected based on Equation (13) and labeled as Pulse 1 and Pulse 2. The relevant parameters of Pulse 1 and Pulse 2 are shown in Table 5. Two sub-models are selected from the third-layer model: the $Transformer3'$ model, trained with time constant ranges of $2 \le \tau_1 \le 2.8$, $12 \le \tau_2 \le 14$, and $50 \le \tau_3 \le 52$; and the $Transformer3''$ model, trained with time constant ranges of $2 \le \tau_1 \le 2.8$, $8 \le \tau_2 \le 10$, and $60 \le \tau_3 \le 62$; the unit for these time constants is μs.

Table 5 Pulse-related parameters

Parameters	Pulse 1	Pulse 2
A(mV)	300	300
$\tau_1(\mu s)$	2.1	2.4
$\tau_2(\mu s)$	12.6	9.2
$\tau_3(\mu s)$	50.8	60.3

The trapezoidal shaping results of distorted Pulse 1 and Pulse 2 are then fed into these two sub-models for analysis. Figure 12 presents a comparison between the original third-order distorted pulses and the pulses identified and restored by each model. Table 6 shows a comparison of the true pulse amplitude parameters and the pulse amplitude parameters identified by each sub-model, before and after incorporating frequency domain analysis (FDA). Before adding FDA, the average relative error of the pulse amplitude coefficients was 1.23%; after incorporating FDA, the average relative error of the pulse amplitude coefficients was reduced to 0.46%. It is evident that the addition of FDA has improved the model's performance, enhancing its parameter identification capabilities compared to before.

Table 6 Comparison of parameters between the original third-order pulse and the identified pulse

	Pulse sequence number	Model	Parameter	True pulse amplitude	Identification value	Relative /%
Before	1	$Transformer\ 3''$	A	300	296.47	1.17
	2	$Transformer\ 3'$	A	300	296.16	1.28
After	1	$Transformer$ +FDA	A	300	298.43	0.52
	2	$Transformer$ +FDA	A	300	298.78	0.40

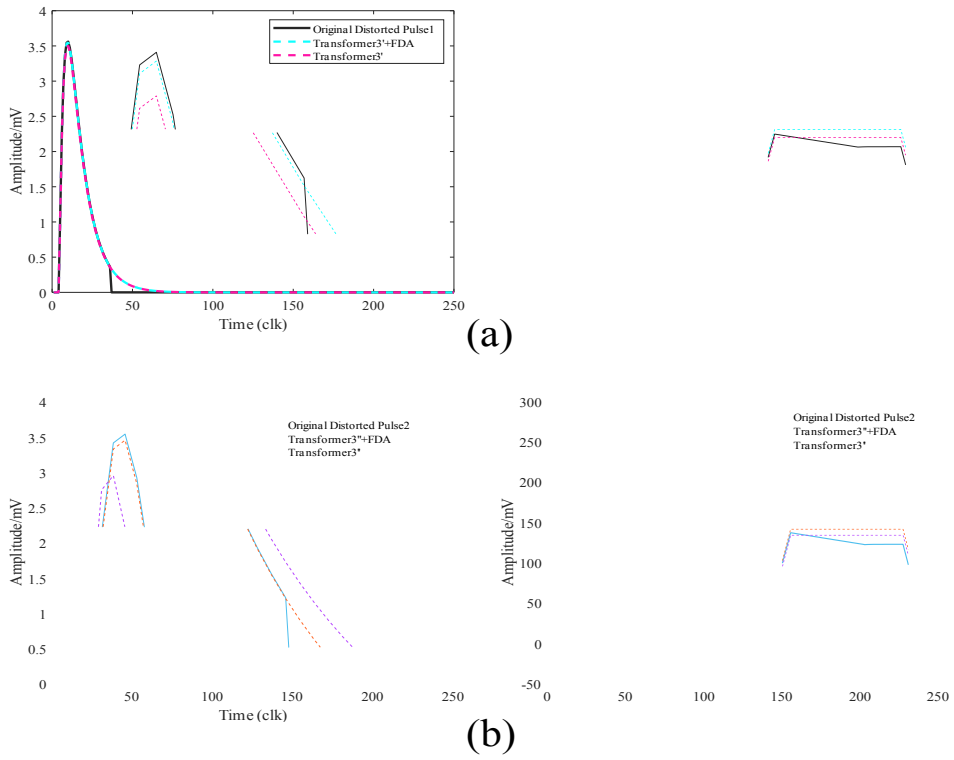

Figure 12 Comparison of the original third-order distortion pulse and the pulse after recognition and restoration

3.7 Energy spectrum correction experimental analysis

3.7.1 Qualitative analysis

To comprehensively and deeply evaluate the effectiveness of the combined method of frequency domain analysis (FDA) and Transformer model in distorted pulse correction, as well as its optimization and improvement for energy spectrum analysis, copper ore samples were selected as the research object in this experiment. The measurement system included a high-performance Silicon Drift Detector (FAST-SDD) and an X-ray tube. The detector was a FAST-SDD detector produced by Amptek, with the model number FAST-RC101. The data acquisition board, featuring a 20MHz 14bit ADC, was developed by Xinxianda Measurement and Control Technology Co., Ltd. The current of the X-ray tube could be adjusted within the range of 3.9uA to 1000uA, and the voltage could be adjusted within the range of 0 to 50kV. Through the analysis of the measurement results, we obtained the X-ray spectrum, as shown in Figure 13. The black spectrum in the figure reveals the presence of unknown shadow peaks preceding the characteristic peaks with higher count rates, in the absence of any correction. It is speculated that these shadow peaks are caused by the phenomenon known as count drift. Count drift refers to the loss of amplitude that occurs during the trapezoidal shaping of distorted pulses, leading to the transfer of counts originally assigned to the characteristic peak region to the shadow peak region. This results in the formation of prominent shadow peaks on the left side of the characteristic peaks.

The existence of these shadow peaks poses a significant risk of being mistaken for characteristic peaks of certain elements, thereby directly affecting the accurate analysis of element content. Therefore, it is crucial to correct the shadow peaks in the energy spectrum. During the correct process, we first processed the trapezoidal shaping results of the distorted pulses using a pre-trained model. Then, we replaced the amplitudes of the original distorted pulses with the amplitudes estimated by the model for the trapezoidal pulses. After this series of processing steps, we obtained optimized results, as indicated by the red spectrum in Figure 13, where the shadow peaks were effectively corrected. Figure 13 presents a comparison of the spectrum before and after the correction of the shadow peaks, demonstrating the efficacy of the proposed method that combines frequency domain analysis with the Transformer model in correcting shadow peaks induced by pulse distortion.

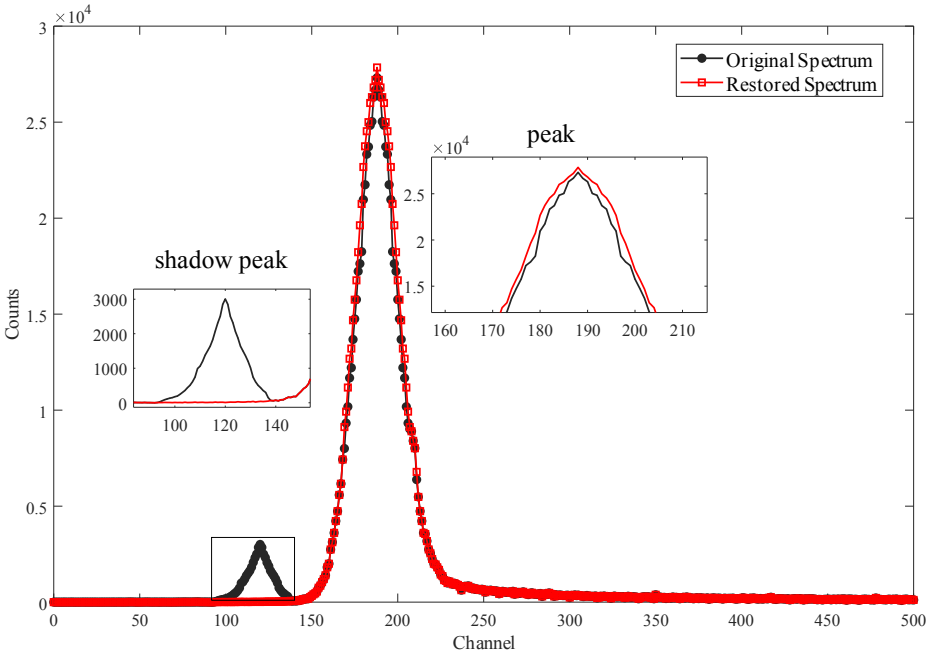

Figure 13 Comparison of the effect before and after the restoration of the shadow peak

3.7.2 Quantitative analysis

As mentioned earlier, the loss of amplitude in distorted pulses leads to count drift, resulting in the formation of a shadow peak on the left side of the characteristic peak. To quantitatively analyze the restoration effect of the energy spectrum counts, we use the peak area (Area) to represent the total count within a specific channel range. Therefore, the analysis of the energy spectrum count restoration results can be transformed into an analysis of the restoration ratio of the peak area. The following is the formula for calculating the peak area:

$$Area_{shadow} = \sum_{i=92}^{140} Counts_{(shadaw-original)} - \sum_{i=92}^{140} Counts_{(shad}$$

$$Area_{peak} = \sum_{i=162}^{212} Counts_{(peak-restored)} - \sum_{i=162}^{212} Counts_{(peak-original}$$

In the equation: $Area_{shadow}$ denotes the count of the restored portion of the shadow peak after implementing spectral peak correction using the model, as depicted in Figure 14a. It is numerically equivalent to the difference in peak area within the channel address interval 92-140, where the shadow peak resides, before and after the spectral peak correction. $Area_{peak}$ represents the count of the restored portion of the characteristic peak after implementing spectral peak correction using the model, as illustrated in Figure 14b. It is numerically equal to the difference in peak area within the channel address interval 162-212, where the characteristic peak is located, before and after the spectral peak correction.

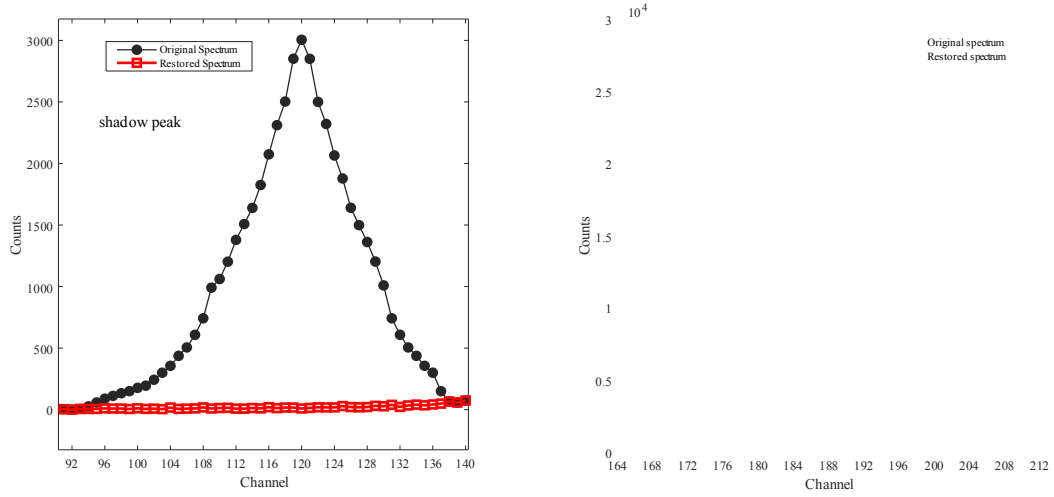

(a) (b)

Figure 14 Comparison of the spectral lines before and after correction

In order to better analyze the model, an index R is introduced to quantify the model's performance. R represents the proportion of shadow peaks that the model corrects, which is numerically equal to the ratio of the difference in peak areas between the address intervals where the feature peaks are located before and after the model is applied to the peak area of the shadow peak generated by the distortion pulse. The calculation is as follows: $$R = \frac{Area_{peak}}{Area_{shadow}} \times 100\% (41)$$

Due to the randomness of radioactive measurements and the inevitable statistical errors in the measurement process, there may be some variation in the correction ratio of the shadow peak. Therefore, in this paper, five experiments were performed on the sample and the resulting discrete trapezoidal pulse sequences were used as input to the model. The pulse amplitudes identified by the model were then used to replace the original pulse amplitudes and the results were analyzed using formulae (39), (40) and (41) as shown in Table 7.

Table 7 Measurement results

	$Counts_{(shadaw-original)}$	$Counts_{(shadaw-restored)}$					
	$Counts_{(peak-original)}$	$Counts_{(peak-restored)}$					
	$Area_{shadow}$	$Area_{peak}$	R(%)				
1	48,006	967	776,279	820,992	47,039	44,713	95.02
2	47,947	1013	778,024	821,916	46,934	43,892	93.52

3	48,212	875	776,957	822,037	47,337	45,080	95.23
4	47,971	842	776,964	821,472	47,129	44,508	94.43
5	48,078	952	777,051	821,135	47,182	44,084	93.54
Average	48,042.8	929.8	777,055	821,510.4	47,213	44,455.4	94.15

From the measurement results presented in Table 7, it is evident that the corrected spectra obtained through pulse amplitude recognition using the Transformer model exhibit two notable characteristics. Firstly, the area of the characteristic peaks has increased compared to the original spectra. Secondly, there is a significant reduction in the area of the shadow peaks. According to the principle of count drift, the area of the shadow peaks should be close to the area increment of the characteristic peaks restored after pulse parameter identification by the model. The effectiveness of the model's correction is evaluated using the R-indicator, and as shown in the table, approximately 94.15% of the shadow peak area can be corrected into characteristic peaks. This holds great significance for improving the accuracy of radioactive measurements.

4 Conclusion

To solve the problem of complex and distorted output signals from the front-end analogue system in nuclear pulse signal detection, this paper proposes a pulse distortion correction method that combines frequency domain analysis with the transformer model. By using frequency domain analysis, the property and initial values of the components contained in the pulse signal are obtained. Then, based on the characteristics of the pulse components and initial parameters, different transformer models are trained to identify the relevant parameters of the distorted pulses. Simulations were performed to compare the relative error of the models in identifying the pulse amplitudes before and after incorporating the frequency domain analysis. The results indicate that the relative error of the model is reduced by approximately 0.8% after the integration of the frequency domain analysis. This result verifies the effectiveness and accuracy of the proposed method in correcting distorted pulses.

In the experiment, we performed five X-ray measurements on a copper ore sample using FAST-SDD and processed the pulses using trapezoidal shaping and multi-channel pulse amplitude analysis. Finally, an X-ray energy spectrum corrected for shadow peaks was obtained. The experimental results show that the proposed model successfully identifies the amplitude parameters of the measured pulse sequences. Meanwhile, using the original energy spectrum obtained without invoking the model as a reference, a comparison with the corrected energy spectrum shows that approximately 94.15% of the shadow peaks can be corrected to characteristic peaks. This is of great importance for improving the completeness and resolution of the X-ray energy spectrum count.

In summary, the distortion pulse restore method proposed in this paper, which is based on frequency domain analysis and the Transformer model, offers a novel approach to addressing nuclear pulse distortion issues. Furthermore, this method demonstrates significant potential in improving the accuracy and resolution of energy spectrum counting, highlighting its important application prospects.

References

[1] H.Q. Zhang, Z.D. Li, B. Tang et al., Optimal parameter choice of CR-RC^m digital filter in nuclear pulse processing. Nucl. Sci. Tech. **30**, 108 (2019). https://doi.org/10.1007/s41365-019-0638-7

[2] M.Y. Kantor, A.V. Sidorov, Detection of true Gaussian shaped pulses at high count rates. J. Instrum. **15**, P06015 (2020). https://doi.org/10.1088/1748-0221/15/06/P06015S. Usman,

[3] A. Patil, Radiation detector deadtime and pile up: a review of the status of science. Nucl. Eng. Technol. **50**(10), 1006–1016 (2018). https://doi.org/10.1016/j.net.2018.06.014

[4] V.T. Jordanov, K.V. Jordanova, Unfolding-synthesis technique for digital pulse processing, part 2: synthesis. Nucl. Instrum. Meth. A **1044**, 167421 (2022). https://doi.org/10.1016/j.nima.2022.167421

[5] W.G. Song, L.J. Zhang, G.Y. Wang, A method to restrain parameter drift in trapezoidal pulse shaping. IEEE Trans. Nucl. Sci. **67**, 1710–1714(2020). https://doi.org/10.1109/TNS.2020.2995901

[6] M. Wang, J.B. Zhou, X.P. Ouyang et al., Gaussian shaper for nuclear pulses based on multilevel cascade convolution. Nucl. Sci. Tech. **33**, 160 (2022). https://doi.org/10.1007/s41365-022-01145-4

[7] H.Q. Huang , X. F. Yang , W.C. Ding et al,. Estimation method for parameters of overlapping nuclear pulse signal. Nucl. Sci. Tech. **28**.1(2017). https://doi.org/10.1007/s41365-016-0161-z

[8] M.S. El-Tokhy, Rapid and robust radioisotopes identification algorithms of X-Ray and gamma spectra. Measurement **168**, 108456 (2021). https://doi.org/10.1016/j.measurement.2020.108456

[9] J. Griffiths, S. Kleinegesse, D. Saunders et al., Pulse shape discrimination and exploration of scintillation signals using convolutional neural networks. Mach. Learn. Sci. Technol. **1**, 045022 (2020). https://doi.org/10.1088/2632-2153/abb781

[10] A. Regadio, L. Esteban, S. Sanchez-Prieto, Unfolding using deep learning and its application on pulse height analysis and pile-up management. Nucl. Instrum. Meth. A **1005**, 165403 (2021). https://doi.org/10.1016/j.nima.2021.165403

[11] B. Jeon, S. Lim, E. Lee et al., Deep learning-based pulse height estimation for separation of pile-up pulses from NaI (Tl) detector. IEEE Trans. Nucl. Sci. **69**, 1344–1351 (2021). https://doi.org/10.1109/TNS.2021.3140050

[12] M. Gomez-Fernandez, W.K. Wong, A. Tokuhiro et al., Isotope identification using deep learning: an explanation. Nucl. Instrum.Meth. A **988**, 164925 (2021). https://doi.org/10.1016/j.nima.2020.164925

[13] C.H. Kim, S. Ahn, K.Y. Chae et al., Noise signal identification in time projection chamber data using deep learning model. Nucl. Instrum. Meth. A **1048**, 168025 (2023). https://doi.org/10.1016/j.nima.2023.168025

[14] M. Touch, D.P. Clark, W. Barber et al., A neural network-based method for spectral distortion correction in photon counting X-ray CT. Phys. Med. Biol. **61**(16), 6132–6153 (2016). https://doi.org/10.1088/0031-9155/61/16/6132

[15] L. Tang, X.K. Ma, K.B. Shi et al., A method for correcting characteristic X-ray net peak count from drifted shadow peak. Nucl. Sci. Tech. **34**, 175 (2023). https://doi.org/10.1007/s41365-023-01333-w

[16] Holl, P., Hauertmann, L., Majorovits, B. et al. Deep learning based pulse shape discrimination for germanium detectors. Eur. Phys. J. **C 79**, 450 (2019). https://doi.org/10.1140/epjc/s10052-019-6869-2

[17] Q. T.Wang, H.Q. Huang, X.K. Ma, et al.,Trapezoidal pile-up nuclear pulse parameter identification method based on deep learning transformer model. Appl. Radiat. Isot. **190**, 110515 (2022). https://doi.org/10.1016/j.apradiso.2022.110515.

[18] Ai, P., Deng, Z., Wang, Y., Shen, C., Universal uncertainty estimation for nuclear detector signals with neural networks and ensemble learning. J. Instrum. **17**,(2021). https://doi.org/10.48550/arXiv.2110.04975

[19] X.K. Ma, H.Q. Huang, X. Ji et al., X-ray spectra correction based on deep learning CNN-LSTM model. Measurement 199, 111510 (2022). https://doi.org/10.1016/j.measurement.2022.111510